Published in final edited form as:
Anat Rec A Discov Mol Cell Evol Biol. 2006 January ; 288(1): 91–103. doi:10.1002/ar.a.20272.

In vivo Delivery of Fluoresceinated Dextrans to the Murine Growth Plate: Imaging of Three Vascular Routes by Multiphoton Microscopy

Cornelia Farnum[1], **Michelle Lenox**[1], **Warren Zipfel**[2], **William Horton**[3], and **Rebecca Williams**[2]

[1] Department of Biomedical Sciences, Cornell University, Ithaca, New York, 14853

[2] Department of Applied and Engineering Physics, Cornell University, Ithaca, New York, 14853

[3] Shriner's Hospital for Children, Portland, Oregon, 97239

Abstract

Bone elongation by endochondral ossification occurs through the differentiation cascade of chondrocytes of cartilaginous growth plates. Molecules from the systemic vasculature reach the growth plate from three different directions: epiphyseal, metaphyseal, and via a ring vessel and plexus associated with the perichondrium. This study is an analysis of the real-time dynamics of entrance of fluoresceinated tracers of different molecular weights into the growth plate from the systemic vasculature, and tests the hypothesis that molecular weight is a key variable in the determination of both the directionality and the extent of tracer movement into the growth plate. Multiphoton microscopy was used for direct in vivo imaging of the murine proximal tibial growth plate in anesthetized 4-5-week-old transgenic mice with green fluorescent protein linked to the collagen II promoter. Mice were given an intracardiac injection of either fluorescein (332.3 Da), or fluoresceinated dextrans of 3, 10, 40, 70 kDa, singly or sequentially. For each tracer, directionality and rate of arrival, together with extent of movement within the growth plate, were imaged in real time. For small molecules (up to 10 kDa) vascular access from all three directions was observed and entrance was equally permissive from the metaphyseal and the epiphyseal sides. Within our detection limit (a few per cent of vascular concentration) 40 kDa and larger dextrans did not enter. These results have implications both for understanding systemic and paracrine regulation of growth plate chondrocytic differentiation, as well as variables associated with effective drug delivery to growth plate chondrocytes.

Keywords

growth plate; vasculature; multiphoton microscopy; endochondral ossification

Introduction

Bone elongation in children occurs by endochondral ossification in cartilaginous growth plates at the ends of long bones. Chondrocytic differentiation in the growth plate begins with clonal expansion of stem cells, continues during cellular proliferation, and ends with cellular enlargement, followed by death and replacement by bone. The kinetics of chondrocytic activity in each stage and of the regulatory transitions between them determine the rate of

Corresponding author: Dr. Cornelia E. Farnum Department of Biomedical Sciences College of Veterinary Medicine Cornell University, Ithaca New York 14853 telephone: 607 253 3543 fax: 607 253 3541 cef2@cornell.edu.

bone elongation achieved. As in any cellular growth system, nutrients are required to sustain the process, and multiple endocrine and paracrine inputs regulate at each stage. For growth plate cartilage, the role of the extracellular matrix also must be considered, not only as a substantive contributor to elongation per se, but through its potential role as a communication link among chondrocytes of the growth plate, and between growth plate chondrocytes and cells of surrounding tissues such as the perichondrium and adjacent bone (Farnum and Wilsman, 2002; Okazaki and Sandell, 2004; Ortega et al, 2004).

The impetus for the physician John Hunter in the 1700s to study the vascular supply to the growth plate was the same as that of multiple physicians and basic scientists of the 20th and 21st centuries: the vascular supply is critical to the normal functioning of the growth plate, and for determining how the growth plate responds to injury. Trauma that affects vasculature to the growth plate can lead to premature closure, forever compromising the potential of the limb to achieve its appropriate final length. Disruption to the perichondrium can accelerate growth causing limb length discrepancy. By 1889, with the publication of Ranvier's *Traité Technique D'Histologie*, all three blood supplies to the growth plate had been described – epiphyseal, metaphyseal and a ring vessel running in Ranvier's groove, hypothesized to supply nourishment to superficial aspects of the growth plate during growth in width (Ranvier, 1889).

In the last decade, analysis of transgenic and gene-targeted mice has become a powerful approach for the study of endocrine, paracrine and autocrine regulators acting through the chondrocytic differentiation cascade (Karsenty, 2001; McClean and Olsen, 2001; deChrombrugghe et al., 2002; Kronenberg, 2003; Horton, 2003; Davey et al., 2004). However, despite advances in delineating cellular and molecular events that define skeletal growth and its regulatory circuitry, relatively little is known about the physiology of the vascular access that endocrine (and potentially paracrine) regulators require to reach growth plate chondrocytes. This deficit reflects a lack of methods to study growth plate vascular physiology under real time conditions in living animals. The matrix and cellular organization of the growth plate is highly anisotropic at micron spatial scales, and the morphology of the vascular/cartilage interface differs spatially in three directions with respect to growth plate chondrocytes. The perichondrium is highly vascularized and the perichondrial stem cell layer transitions to growth cartilage circumferentially. The epiphyseal chondroosseous junction (COJ), at the junction of the growth plate and the secondary center of ossification, is nearest to the proliferative chondrocytes. The metaphyseal COJ is where hypertrophic chondrocytes die and endothelial cells advance with osteoprogenitor cells to initiate bone formation on the previously calcified cartilaginous matrix.

In this study we apply a novel approach using multiphoton microscopy (MPM) for imaging of access from the systemic vasculature to the murine proximal tibial growth plate. MPM allows imaging under stable physiological conditions, with analysis of delivery of fluoresceinated molecules of different molecular weight to the growth plate in vivo and in real time (Williams et al., 2001; Zipfel et al., 2003a,b; Niell and Smith,2004; Rubart, 2004). Our hypothesis is that tracers of different molecular weight reach the growth plate through different vascular routes, and that they arrive at different times and in different amounts. We propose that this differential behavior reflects potentially different physiological roles of the three vascular access routes during endochondral ossification. Understanding physiological differences among the three routes of vascular access to the growth plate has implications for understanding rate variables regulated through paracrine and systemic pathways during post-natal long bone growth, as well as for developing strategies for effective drug delivery to the growth plate (Miller et al, 2005).

Materials And Methods

In vivo multiphoton microscopy

The multiphoton microscope used has been described previously (Kloppenburg et al., 2000; Zipfel et al., 2003b). The illumination source consisted of a Ti:Sapphire laser (Milenia/Tsunami combination, Spectra Physics, Mountain View, CA) directed into a BioRad MRC 600 laser scanner interfaced with a modified Olympus AX-70 upright microscope. A frequency spread in the output beam was necessary for supporting mode-locked (pulsed) operation and was monitored by a laser spectral analyzer (IST/Rees E201, Horseheads, NY). The excitation light was focused into the growth plate with a large-barrel Olympus 20X/0.95 numerical aperture (NA) water objective, which provided a large field-of-view, a relatively high NA, good infrared transmission, and the few mm of working distance necessary for maneuvering in live animals.

For in vivo imaging of fluoresceinated molecules, the multiphoton illumination wavelength (λex) was tuned to 900 nm (Xu et al., 1996; Zipfel et al., 2003a). Nonlinear emissions were collected in epifluorescence mode and separated from the excitation beam directly after the objective with a 670DCXXRU longpass dichroic (Chroma Technology Inc., Rockingham, VT). Emission filters were chosen for a clean blue, green (450 and 515 nm) separation (BGG22 and 580/150 filters with a separating 500DCXR dichroic, Chroma Technology Inc.) and a 107 rejection ratio of the exciting to emitting wavelengths. The resulting two emission beams were collected by HC125-02 bialkali photomultiplier tube assemblies (Hamamatsu, Bridgewater, NJ). Typically 0.3 Mbyte images were recorded and stored on hard disc using the BioRad MRC 600 image acquisition software.

Gross plate morphology: histological and multiphoton images

Figure 1A depicts a growing long bone, demonstrating the relationship of the three routes of potential vascular access to the murine growth plate. Growth plate regional terminology defines the epiphysis as the region between the growth plate and the joint. In the 4-5 week-old mouse, the epiphysis has a well-developed secondary center of ossification filled with trabecular bone and marrow spaces penetrated by multiple independent epiphyseal vessels. The metaphysis is the bone region distal to the growth plate that continues to reflect the longitudinally directed organization of chondrocytic columns of the growth plate. Blood in the metaphysis is from terminal branches of the primary nutrient artery, which ramifies throughout the bone as the principal blood supply (Brookes, 1971). Figure 1A also depicts a ring vessel joining into a subperichondrial plexus on the hypertrophic cell side of the growth plate.

Figure 1B is a picture of the murine proximal tibial growth plate at four weeks, showing the relationships of the epiphysis with articular cartilage and the secondary center of ossification, the perichondrium, and metaphyseal bone. Figure 1C shows the characteristic zones indicating stages of chondrocytic differentiation – reserve, proliferative, hypertrophic – based on cellular morphology. As shown in Figure 1D, MPM of live, non-stained and non-sectioned tissue allows the same morphological distinctions of cellular zones. For imaging tissue explants using their intrinsic autofluorescence, the illumination wavelength was set to 770 nm, allowing visualization of cellular autofluorescence such as NADH and second harmonic generation from collagen (Zipfel et al., 2003a; Mertz, 2004).

Col II/GFP mice: phenotype identification and preparation for imaging

A Col II reporter mouse was used, with expression of green fluorescent protein (GFP) controlled by the type II collagen promoter/enhancer (Grant et al., 2000; Cho et al., 2002; Gareau et al., 2004). GFP+/- mice were identified at 14 days by observing the fluorescence

of cartilage taken in an ear punch, obviating the need for formal genotyping. Thirty minutes prior to imaging, oxytetracycline (OTC, 10 mg/kg, intraperitoneal (IP)) was given. This calcium chelator labels the chondroosseous junctions (COJs) of the growth plate, and was used as an orientation marker under fluorescence illumination (Hansson, 1967), allowing the use of GFP-/- mice. Using the fluorescence of growth plate GFP-expressing chondrocytes and of OTC-labeled epiphyseal and metaphyseal bone for orientation, we were able to image up to 200 μm deep to the perichondrium.

Choice of growth plate and surgical approach

The ideal growth plate for in vivo imaging would be rapidly growing, easily accessible with minimal overlying muscle, and with a flat contour not obstructed by tendons or ligaments. In this study the medial aspect of the proximal tibial growth plate just caudal to the medial collateral ligament (MCL) was imaged. Figure 2A illustrates the experimental set-up of the mouse lying in dorsal recumbency with the nose positioned in tubing leading to an isoflurane anesthetic system. A two-chamber stage allowed submersion of the limb in lactated Ringer's (LR) for water-immersion imaging. Stabilization of the limb was achieved by pinning the toe webbing through Sylgard®.

An incision was made on the posteriomedial aspect of the left limb and the skin tacked back (2B). Knee level attachments of the biceps femoris muscle were dissected away, revealing the proximal attachments of the gastrocnemius muscle. The saphenous vessels and nerve were retracted caudally (2B). Superficial fascia was removed using a #11 scalpel blade, leaving the joint capsule and perichondrium intact. To position the growth plate caudal to the MCL with the flat area uppermost, a pin was placed caudal to the patellar ligament, and the ligament was rolled cranially. If required, bleeding was controlled with electrocautery. The dissection field was kept moist with LR using a perfusion system and in-line warming (37°C) on the stage. Procedures were approved by the Institutional Animal Care Committee.

Standard imaging protocol

Mice between 4-5 weeks of age were induced in a chamber of isoflurane and weighed. The surgical approach was completed within ~30 minutes. Wide field images were recorded using an Olympus fluorescent dissection microscope (SZX12). Figure 2C is the surgical field, with the imaging area under UV excitation for detection of OTC-fluorescence. The growth plate shows as a non-fluorescent band between yellow-green OTC-fluorescence of the epiphyseal and the metaphyseal bone. Figure 2D is the same specimen under blue illumination demonstrating GFP-fluorescence.

The growth plate is the green band between two regions of non-fluorescing bone. Two asterisks mark the position of the MCL. After the mouse was transferred to the microscope stage, perfusion of LR (37°C) was started.

Positioning was verified by an initial z-series (sequential images through multiple optical planes from superficial to deep) through the perichondrium and into the growth plate, to reference imaging depth. Separation of emission colors allowed simultaneous imaging of collagen, and OTC and GFP-fluorescence. Collagen second harmonic generation allowed orientation to the layers of perichondrium, while OTC and GFP-fluorescence elucidated the architecture of the growth plate (Freund and Deutsch, 1986; Williams et al, 2001; Mertz, 2004). At focal planes further than ~50 μm deep to the perichondrium the epiphyseal and metaphyseal COJs were roughly parallel to each other.

Tracer concentrations

Fluorescein (332.3 Da, Ak-Fluor 25%, Akorn, Decatur, IL) was generally diluted to a 1% (30 mM) stock solution in phosphate buffered saline (PBS). Unless otherwise stated, an IC injection of 50 μl was used, yielding a vascular concentration of ~2 mM. Stock solutions of fluorescein-labeled dextrans of 3, 10, 40 and 70 kDa (Invitrogen) were prepared at 100 mg/ml in PBS. Varying amounts were delivered by IC injection to yield a similar vascular fluorescence to that of fluorescein. At least three replicates were done for each tracer. In several experiments an intraperitoneal (IP) injection of fluorescein was given for comparison to IC delivery. Some experiments used injection of a high molecular weight dextrans followed by a fluorescein injection, as a check on maintenance of vascular integrity, measured by consistency of the pattern of fluorescein entrance.

Data analysis

All data analysis was accomplished using macros written in the IDL image analysis platform (RSI Inc., Boulder, CO). For the arrival time analysis, image series were rotated so that the long axis of the bone was horizontal. Image fluorescence data were averaged transversely across the growth plate to produce a single fluorescence curve per time point. The arrival time was defined as the time at which the position-specific fluorescence reached one half of its five-minute value. Note that by five minutes (after IC injection) the fluorescence within the growth plate no longer increased; we assume at this point the tracer was uniformly distributed within the matrix. By inspection of the z-series acquired for each mouse, heterogeneities in the visual field after tracer equilibration resulted not from absolute differences in tracer incorporation, but from the amount and type of overlying tissue through which the laser beam traveled. Thus, we calculated the arrival half-time relative to the position-specific five-minute fluorescence value, in order to normalize for imaging artifacts due to tissue scattering.

For analyzing the total amount of tracer entering the growth plate, the average growth plate fluorescence was calculated as a percentage of the average fluorescence in the metaphyseal and epiphyseal bone. In absolute terms this is a rough estimate, both because the available extracellular space differs in the three regions (epiphyseal bone, metaphyseal bone, and growth plate) and because more fluorescence emission is scattered out (not detected) from the two bone regions than from the growth plate. However, on a relative scale this analysis offers an accurate comparison among tracers of varying molecular weights.

Results

The ring vessel and plexus surround the hypertrophic cell zone of the growth plate

Figures 3A-D are a series of multiphoton images from a growth plate both GFP-positive and labeled with OTC. They demonstrate four frames from a z-series, from superficial to deep, starting at the superficial edge of the periosteum (A), imaging through the periosteum (B,C), and ending with an image of the growth plate, approximately 50 μm deep to the periosteum (D). Note the arrangement and extent of collagen fibrils of the perichondrium penetrated before reaching the growth plate. At this depth the GFP signal from hypertrophic cells is considerably fainter than that of proliferative cells.

After entrance of fluorescein, and when the blood plasma had become saturated with fluorescein, the extent and complexity of the plexus associated with the ring vessel and the relationship of the ring vessel and plexus to the perichondrium and growth plate could be visualized. Figures 3E-H are four frames of a z-series demonstrating that the plexus is slightly more superficial than the ring vessel (compare E to H), and that both are adjacent to the deepest edge of the perichondrium. Relative to growth plate cellular zones, the ring

vessel is positioned approximately at the P/H junction, and the plexus is entirely on the hypertrophic cell side. Asterisks in EG,H mark the position of the metaphyseal COJ. The plexus and ring vessel also were associated with vessels that parallel the long axis of the bone running in the perichondrium (3G).

Arrival pattern of fluorescein to the growth plate differs with depth of imaging

Each four-frame series in Figure 4 demonstrates a time sequence of arrival of fluorescein into the growth plate. Series A-D is at a focal plane deeper into the growth plate (relative to the ring vessel) than series E-H. Fluorescein is pseudo-colored red, while OTC and GFP-fluorescence are green. Double and single arrowheads at the left of the first picture in each series demarcate the position of the epiphyseal and metaphyseal COJs, respectively. Figures A-D are from a GFP-negative mouse with OTC labeling the bone more brightly on the metaphyseal side where growth is most active. Fluorescein injected IP entered from both the epiphyseal and the metaphyseal sides (C, D), and the two waves of fluorescein met at approximately the P/H junction (D, asterisk). By contrast, when imaging was done more superficially as seen in Figures E-H, the primary source of entrance of fluorescein injected IP was from the ring vessel and plexus. The area just deep to the ring vessel and plexus, from the P/H transition to the metaphyseal COJ, received signal before any signal appeared in the matrix of the proliferative zone (F). Due to the superficial imaging plane the ring vessel makes a shadow, also at the P/H junction (three arrows in G,H).

All three vascular access routes are permissive to entrance of tracers up to 10kDa

The arrival time is defined as the time at which the fluorescence at a given position reached 1/2 of its five-minute value (as described under Methods). Graphs in Figure 5 describe the entrance of fluorescein into the growth plate, with arrival time on the vertical axis plotted against position in the growth plate. The growth plate is oriented with the epiphyseal COJ left and the metaphyseal COJ right. The respective COJs are represented as vertical lines, and a time scale in seconds is shown along the epiphyseal COJ of each image. Fluorescence from an IC injection saturates the growth plate within five minutes. Figure 5A confirms graphically the visual impression of IC fluorescein entrance into the growth plate as seen in Figures 4A-D – simultaneously and instantaneously, and to the same extent from both the epiphyseal and the metaphyseal directions. Figure 5B demonstrates the form of the graph when imaging is done in a superficial position capturing entrance from the ring vessel, analogous to Figures 4E-H. In 5B the lower flat plateau of the graph at the P/H junction (small arrow) indicates that fluorescein enters the P/H junction first from the ring vessel, before it reaches the P/H junction from either the epiphyseal or the metaphyseal vasculatures.

Figures 5C,D and Figures 5E,F are comparable graphs for the entrance of the 3 kDa and 10 kDa dextrans, respectively. After IC injection, intense fluorescence was detected essentially instantaneously in both the epiphyseal and metaphyseal vasculatures. Entrance of the 3 kDa dextran mirrored that of fluorescein, as shown in graphs imaged deep and superficial in the growth plate (C,D respectively). This pattern was similar for 10 kDa dextran (E,F). There was no detectable entrance of either the 40 kDa (G) or 70 kDa dextran (data not shown). The only difference between IP and IC injections of fluorescein was in the absolute time the tracer left the vasculature to enter the growth plate. IC injections delivered fluorescein instantaneously to the growth plate from the vasculature (A,B); first detectable arrival from IP injections was as late as ~130 seconds (H), because filling of the vasculature was signficantly slower following an IP injection.

The relative amount of tracer entering the growth plate from the vasculature decreases with increasing molecular weight

The graph in Figure 6 gives a quantitative estimate of fluorescence reaching into the growth plate, relative to that in the adjacent metaphysis and epiphysis. This estimate is only roughly accurate, because bone is significantly more scattering than cartilage so that detected signal from the metaphysis and epiphysis will be somewhat reduced compared to that from the growth plate. However, relative comparisons are appropriate. Fluorescein, injected either IP or IC, diffused into the growth plate to levels comparable to those in the vasculature. Levels of the 3 kDa dextran were only ~60% of that in the vasculature, and levels of the 10 kDa dextran were only approximately a tenth. The amount of dextran entering the growth plate decreased sharply with increasing molecular weight with no detectable entry from dextrans of 40 kDA and greater.

Tracer from either COJ can access the full length of the growth plate

The question arises whether particular vasculatures only feed certain zones within the growth plate. In some experiments, the arrival of a given tracer into the epiphyseal or metaphyseal vasculature was significantly delayed after IC injection. With tracer only in the epiphyseal vasculature (7A), fluorescein moved from the epiphyseal side throughout the growth plate to the metaphyseal COJ. If the metaphyseal vasculature filled with fluorescein more rapidly than the epiphyseal vasculature (9B), the opposite occurred. Figure 7B demonstrates movement of fluorescein from the metaphyseal side reaching beyond the P/H junction and into the proliferative cell zone, before it meets fluorescein that initially entered from the epiphyseal side. Dextrans of 3 kDa and 10 kDa behaved similarly. In Figure 7C the 10 kDa dextran entered primarily from the metaphyseal vasculature and traveled through the growth plate well into the proliferative zone. Fluorescein injected into the same mouse following the 10 kDa injection mirrored the same pattern (7D). Thus the extent of tracer movement within the growth plate depended primarily on the difference in time of its initial arrival into either the epiphyseal of the metaphyseal vasculatures, and there did not appear to be any diffusional blocks within the growth plate itself.

Discussion

The dual nature of the epiphyseal and metaphyseal vasculatures is not due to an access difference from the two vasculatures

Over forty years ago, Joseph Trueta presented results of studies on the effect of ischemia on the growth plate, experimentally induced by compromising parts of either epiphyseal or metaphyseal blood routes (Trueta, 1963; Trueta, 1968). When epiphyseal vessels were compromised, chondrocytes at all levels of the growth plate died. When metaphyseal vessels were compromised, chondrocytes did not die, but there was failure of replacement of cartilage by bone at the metaphyseal COJ. From these results a conclusion was drawn that remains the primary generalization on the dual nature of the epiphyseal and metaphyseal blood supplies to the growth plate: the epiphyseal supply is the nutrient supply for the entire growth plate, and the metaphyseal supply is essential for signaling death of the terminal chondrocyte followed by bone deposition on the calcified cartilage.

We directly tested Trueta's hypotheses by examining the physiological basis of access from each vascular compartment. Our initial hypothesis was that, in positions distant from the superficial edge of the growth plate, entrance would be primarily from the epiphyseal side, consistent with Trueta's observations supporting the role of the epiphyseal vasculature for nutrient delivery throughout the growth plate. We also hypothesized that molecules involved in paracrine interactions for turnover at the metaphyseal chondroosseous junction would not require significant movement into the growth plate itself. Our results indicate that the small

molecule fluorescein enters with equal facility from both the epiphyseal and metaphyseal sides, as do the 3 kDa and 10 kDa dextrans. These observations do not support our original hypotheses but suggest an alternative hypothesis that molecules of low molecular weight, such as basic nutrients and systemic hormones of 10 kDa or less, potentially have access from the systemic vasculature to the growth plate equally from both directions. The directionality of their entrance at any given time may rely primarily upon their concentrations within each vascular route, the flow velocity within individual vessels, and whether molecules are being delivered systemically or through venous/arterial anastomoses from adjacent tissues (Ginther, 1974).

Biomolecular size exclusion of dextrans equal or greater than 40 kDa

There is a broader question of the size limitation for transport of plasma soluble constituents into growth plate ECM, and the extent to which this may vary in the epiphyseal and metaphyseal directions based upon specific physiological properties of the endothelial cells themselves. There is a wide range of molecular weight for systemic and paracrine regulators of the growth plate differentiation cascade, from less than 500 Da for nutrients such as glucose and systemic hormones such as thyroxine and sex steroids, to greater than 50 kDa for matrix metalloproteinases (Ballock and O'Keefe, 2003). The question of the presence of endothelial barriers based upon size, as well as the presence/absence of transport systems allowing differential rates and entrance of molecules based on the selectivity of specific receptors, is significant. For endothelia of several organs of the body experimental evidence points to the existence of what has been referred to as two sets of physiological pores – large pores responsible for the transport of proteins and small pores designed for the diffusion of small solutes. Opinions differ widely concerning which features of endothelial cells found in these organs – fenestrae, the trans tubulo-vesicular system including caveolae, and inter-endothelial clefts – are the morphological correlates to the two pore system suggested by the physiological data (Predescu et al, 1997; Michel and Curry, 1999; Silverstein, 1999; Smart et al., 1999; Galbiati et al., 2001; Bendayan, 2002; Feng et al., 2002; Simionescu et al., 2002).

This level of analysis, from either the morphological or the physiological perspective, has not been done for the vasculature surrounding growth plate cartilage. Nevertheless, two observations separated by almost four decades are particularly relevant. First, carbon black injected into the systemic vasculature of a rat localizes to the metaphyseal COJ (Ham et al., 1965). Here metaphyseal capillaries lack a basement membrane and are leaky, even to high molecular weight, non-physiological, molecules such as carbon black. This implies that at the metaphyseal COJ essentially no barriers for exiting endothelial lumina based upon molecular size exist, or, if they exist, they reside in the macromolecular structure and composition of the growth plate extracellular matrix. Second, recent experiments indicate that perlecan is found in epiphyseal and perichondrial vessels of growing long bones, but not in metaphyseal vessels (Melrose et al., 2004). This provides evidence supporting unique structural differences of metaphyseal vessels, compared to vessels of either the perichondrium or the epiphysis, which may have a role in the differential selective permeability of these vessel systems to molecules of different sizes.

MPM imaging allows morphological definition of the sub-perichondrial ring vessel and its associated plexus in the living animal

This study has added significant observations concerning vascular access to the growth plate, building upon an already extensive literature. Starting in the 1950s injection methods allowed visualization by microradiography and scanning electron microscopy. Morgan (1959) and others demonstrated the complexity of branching patterns of vessels in the epiphysis and metaphysis, confirming metaphyseal arterial vessels terminate proximal to the

COJ, and that vessels closest to the cartilage are an irregular and dilated sinusoidal venous network of closed loops (reviewed by Brookes, 1971; Brighton, 1978; Kuettner and Pauli, 1983). Morgan also demonstrated that a ring vessel feeds into a lattice-work plexus positioned asymmetrically over the distal 1/2 of the growth plate (hypertrophic zone cartilage), making connections to both the metaphyseal and epiphyseal circulations (Morgan, 1959; Irving, 1964). Analyses using scanning electron microscopy of corrosion casts have allowed a third dimension to visualization, but have not challenged the basic concept of the termination pattern of vasculature routes associated with the growth plate (Arsenault, 1987; Hunter and Arsenault, 1990; Stanka et al.,1991; Aharinejad et al., 1995; Komuta, et al., 1998, as examples).

In the current study, the positional morphology and extent of the vascular plexus associated with the ring vessel has been described in considerably more detail than previously with four significant observations: 1) the ring vessel encircles the growth plate just deep to the perichondrium at the level of the P/H junction; 2) the associated plexus is entirely on the hypertrophic cell side of the growth plate, continuing to surround the metaphyseal COJ; 3) both the plexus and the ring vessel are deep to the perichondrium, in direct contact with the cartilage of the growth plate; 4) in the murine growth plate, tracers can diffuse from the ring vessel and plexus at least 75 μm into the growth plate and diffusion from this vessel is more rapid to this point than from either the epiphyseal or the metaphyseal side.

This allows the speculation that the ring vessel and its plexus may be involved in paracrine regulation via the vasculature to the growth plate from the perichondrium, such as been demonstrated for uterine/ovarian reciprocal regulatory pathways (Ginther, 1974). The Ihh/PTHrP negative feedback loop acts to “put the brakes on” at the junction between the end of proliferation and the initiation of hypertrophy, requiring communication between growth plate chondrocytes and the perichondrium (Vortkamp et al., 1996; Long and Linsenmayer, 1998; Pathi et al., 1999; Volk and Leboy, 1999; Pateder et al., 2000; DiNino et al., 2002; Allen et al., 2004). Recent studies provide data that vascular endothelial growth factor (VEGF) alters the permeability characteristics of the vascular endothelium in paracrine regulation of the growth plate involving the perichondrium (Roberts and Palade, 1995; Esser et al., 1998; Ericksson et al, 2003; Cao et al., 2004), Zelzer et al, 2002; Aramoto et al., 2004; Zelzer and Olsen, 2005). VEGF's more established role for paracrine regulation exists at the metaphyseal COJ, where it is produced by hypertrophic chondrocytes, and here VEGF may be responsible for the extreme vascular permeability to the surrounding bone matrix (Vu et al., 1998; Gerber et al., 1999; Gerber and Ferrara, 2000; Aramoto et al., 2004).

The role of the ring vessel and its plexus in these communication loops essentially is unknown, primarily because there has not been an experimental approach for analysis of the physiological role of this route of vascular access to the growth plate in vivo. Future studies using MPM imaging of the ring vessel and the plexus have the potential to analyze entrance of specific physiological regulators through these routes and their movement between the perichondrium and the P/H junction of the growth plate.

Experimental issues related to the use of dextrans as molecular tracers in the study of vascular morphology and physiology of the growth plate

Dextrans are a standard tracer molecule to study non-selective transport that is neither active nor mediated by specific receptors across the vascular barrier (Simionescu et al., 1972, 2002; Heinzmann, 1980; Thorball, 1981). Their positive attributes are that they are stable, highly soluble, non-toxic, non-charged at the pH of normal blood, of biological origin, and available in a wide range of molecular weights (Thorball, 1981). Dextrans are surrogates for biological molecules of interest and the only variable they test is difference based on molecular weight. From our current data it is not possible to exclude the possibility that

regulators of growth plate function of 40 kDa and greater (such as MMPs, VEGFs, and TGF-β) behave differently in their ability to enter and travel within the growth plate, than that demonstrated by dextrans used as surrogates.

An insidious problem with the use of dextrans is that they may interact with vessel walls and change the functional properties of the endothelium or cause changes in blood viscosity (Gustafsson et al., 1981; Pearson and Lipowsky, 2000; Bendayan, 2002; Gonzalez-Castillo et al., 2003; Tsai et al., 2003). Specifically, dextrans can bind irreversibly to the coronary vessel lumen in a mass-dependent manner and modulate coronary blood flow (Gonzalez-Castillo et al., 2003). Dextrans >100 kDa have been shown to alter the level of leukocyte adhesion to the endothelial lumen (Pearson and Lipowsky, 2000; Tsai et al., 2003; Kamler et al., 2004). In our experiments the rate and directionality of fluorescein movement following dextran injections did not differ from that seen pre-injection, giving assurance that the fundamentals of flow within the vessels had not been altered by the dextran injection.

Extent of movement of a tracer within the growth plate depends upon directionality of initial departure from the vasculature

In some experiments where the tracer (be it fluorescein or a dextran) failed to reach the epiphyseal or metaphyseal vasculatures simultaneously after IC injection, the tracer still reached the full extent of the growth plate. While it is not clear whether these cases represent a normal physiological situation, they do suggest an interesting hypothesis that the *extent of availability* within the growth plate of fluorescein and 3 kDa and 10 kDa dextrans depends less upon rates that they leave the vasculature, and more on *their initial availability* in a specific vascular compartment: epiphyseal, metaphyseal or perichondrial. While in our experiments this may have been the result of a transient redirection of blood flow due to the experimental procedure, the situation could mirror one where concentration levels in a specific vascular compartment are the result of a paracrine regulatory loop (substance produced in the perichondrium, delivered to the perichondrial vessel and plexus and then entering into the growth plate), or a venous/arterial anastomosis (substance produced in the metaphyseal bone, delivered to the metaphyseal venous system, anastomosis to the perichondral ring vessel and then enters the growth plate). It is only through detailed analyses of blood flow throughout the three vascular supplies to the growth plate that meaningful data can be collected to test this hypothesis by analyzing whether local vascular portal routes are significant in the paracrine regulatory pathways operating during the chondrocytic differentiation cascade.

Caveats to the interpretation of MPM images in these experiments

There are caveats to the interpretation of images generated from MPM (Williams et al., 2001; Zipfel et al., 2003b). The image at a given focal plane is affected by the nature of the material penetrated in all regions superficial to it. In our experiments the perichondrium was intact, leaving a significant collagenous barrier (~50-100 μm) the beam must penetrate before reaching the growth plate. Since chondrocytes just deep to the perichondrium are involved primarily with growth in width, it is necessary to image through these to access focal planes of chondrocytes involved primarily in longitudinal growth. Because of the anisotropic spatial characteristics of the growth plate, and also because epiphyseal and metaphyseal bone vary significantly in their trabecular orientation, the ability of the laser to penetrate is not the same across the entire section being imaged. Superficial vasculature, including the ring vessel and the plexus, forms imaging shadows over deeper structures, which is another source of non-homogeneity of imaging across one focal plane. Superficial bleeding is incompatible with good imaging, but fortunately was not a problem.

Summary

Our study has achieved, for the first time, an analysis in vivo and in real time of three “entrance” variables (amount, rate, direction) for molecules of a range of molecular weight of physiological relevance as they move from the vasculature into the growth plate. Rate of entrance and potential directionality of entrance from a systemic injection did not differ for fluorescein and the 3 kDa and 10 kDa dextrans. The most significant variable for determining the directionality of entrance of these tracers was their level of availability in each vascular compartment. Movement within the growth plate was shown to be equally permissive from either the metaphyseal or the epiphyseal side. When put together with Trueta's observations on the dual nature of the epiphyseal and metaphyseal vasculatures, and current knowledge of systemic and paracrine regulation within the growth plate, these observations would suggest availability within a specific vascular compartment, and not the permeability of the compartment itself, determines directionality of entrance of nutrients and molecular regulators of this size during the differentiation cascade of growth plate chondrocytes.

Acknowledgments

The authors wish to thank Vicki Meyers-Wallen for consultation about the surgical procedure, and Robin Gleed, Timothy Damron, Jill Urban and Robert Gilmour for helpful conversations. Thanks also to Linda Jones and Kriss Eckenrode with help in preparing the bibliography.

Grant Sponsor National Institutes of Health 1 RO1 AR 052003-01 Shriner's Hospital for Children, Portland, Oregon

Literature Cited

Aharinejad S, Marks SC Jr, Böck P, MacKay CA, Larson E, Tahamtani A, Mason-Savas A, Firbas W. Microvascular pattern in the metaphysis during bone growth. Anat Rec. 1995; 242:111–122. [PubMed: 7604975]

Allen MR, Hock JM, Burr DB. Periosteum: biology, regulation, and response to osteoporosis therapies. Bone. 2004; 35:1003–1012. [PubMed: 15542024]

Aramoto H, Breslin JW, Pappas PJ, Hobson RW, Durán WN. Vascular endothelial growth factor stimulates differential signaling in *in vivo* microcirculation. Am J Physiol Heart Circ Physiol. 2004; 287:H1590–H1598. [PubMed: 15155260]

Arsenault AL. Microvascular organization at the epiphyseal-metaphyseal junction of growing rats. J Bone Miner Res. 1987; 2:143–149. [PubMed: 3455163]

Ballock RT, O'Keefe RJ. Current concepts review: the biology of the growth plate. J Bone Joint Surg. 2003; 85-A:715–726. [PubMed: 12672851]

Bendayan M. Morphological and cytochemical aspects of capillary permeability. Micros Res Tech. 2002; 57:327–349.

Brighton CT. Structure and function of the growth plate. Clin Orthop Relat Res. 1978; 136:22–32. [PubMed: 365420]

Brookes, M. The Blood Supply of Bone: An Approach to Bone Biology. London: Butterworth Company; 1971. Growth Cartilages; p. 133-161.

Cao R, Eriksson A, Kubo H, Alitalo K, Cao Y, Thyberg J. Comparative evaluation of FGF2-, VEGF-A-, and VEGF-C-induced angiogenesis, lymphangiogenesis, vascular fenestrations, and permeability. Circ Res. 2004; 94:664–670. [PubMed: 14739162]

Cho JY, Grant TD, Lunstrum GP, Horton WA. Col 2- GFP reporter mouse- A new tool to study skeletal development. Am J Med Genet. 2002; 106:251–253. [PubMed: 11891675]

Davey RA, MacLean HE, McManus JF, Findlay DM, Zajac JD. Genetically modified animal models as tools for studying bone and mineral metabolism. J Bone Miner Res. 2004; 19:882–892. [PubMed: 15125787]

deCrombrugghe, B.; Lefebvre, V.; Nakashima, K. Deconstructing the molecular biology of cartilage and bone formation. In: Rossant, J.; Tam, PPL., editors. Mouse Development: Patterning, Morphogenesis, and Organogenesis. San Diego: Academic Press; 2002. p. 279-295.

Di Nino DL, Crochiere ML, Linsenmayer TF. Multiple mechanisms of perichondrial regulation of cartilage growth. Dev Dynam. 2002; 225:250–259.

Eriksson A, Cao R, Roy J, Tritsaris K, Wahlestedt C, Dissing S, Thyberg J, Cao Y. Small GTP-binding protein rac is an essential mediator of vascular endothelial growth factor-induced endothelial fenestrations and vascular permeability. Circulation. 2003; 107:1532–1538. [PubMed: 12654612]

Esser S, Wolburg H, Breier G, Kurzchalia T, Risau W. Vascular endothelial growth factor induces endothelial fenestrations in vitro. J Cell Biol. 1998; 140:947–959. [PubMed: 9472045]

Farnum, CE.; Wilsman, NJ. Chondrocyte kinetics in the growth plate. In: Shapiro, IM.; Boyan, B.; Anderson, HA., editors. The Growth Plate. Washington DC: IOS Press; 2002. p. 245-257.

Feng D, Nagy JA, Dvorak HF, Dvorak AM. Ultrastructural studies define soluble macromolecular, particulate, and cellular transendothelial call pathways in venules, lymphatic vessels, and tumor-associated microvessels in man and animals. Microsc Res Tech. 2002; 57:289–326. [PubMed: 12112440]

Friedl P. Dynamic imaging of cellular interactions with extracellular matrix. Histochem Cell Biol. 2004; 122:183–190. [PubMed: 15258769]

Freund I, Deutsch M. 2nd-harmonic microscopy of biological tissues. Opt Lett. 1986; 11:94–96. [PubMed: 19730544]

Galbiati F, Razani B, Lisanti MP. Emerging themes in lipid rafts and caveolae. Cell. 2001; 106:403–411. [PubMed: 11525727]

Gareau D, Bargo P, Horton W, Jacques S. Confocal fluorescence spectroscopy of subcutaneous cartilage expressing green fluorescent protein versus cutaneous collagen autofluorescence. J Biomed Opt. 2004; 9:254–258. [PubMed: 15065888]

Gerber HP, Vu TH, Ryan TH, Kowalski AM, Werb Z. VEGF couples hypertrophic cartilage remodeling, ossification, and angiogenesis during endochondral bone formation. Nat Med. 1999; 5:623–629. [PubMed: 10371499]

Gerber HP, Ferrara N. Angiogenesis and bone growth. Trends Cardiovas Med. 2000; 10:223–228.

Ginther OJ. Internal regulation of physiological processes through local venoarterial pathways: a review. J Anim Sc. 1974; 39:550–564. [PubMed: 4213194]

Gonzalez-Castillo C, Rubio R, Zenteno-Savin T. Coronary flow-induced inotropism is modulated by binding of dextrans to the endothelial luminal surface. Am J Physiol Heart Circ Physiol. 2003; 284:H1348–H1357. [PubMed: 12511428]

Grant TD, Cho J, Arial KS, Weksler NB, Smith RW. Col2- GFP reporter marks chondrocyte lineage and chondrogenesis during mouse skeletal development. Dev Dynam. 2000; 218:394–400.

Gustafsson L, Appelgren L, Myrvold HE. Effects of increased plasma viscosity and red blood cell aggregation on blood viscosity in vivo. Am J Physiol Heart Circ Physiol. 1981; 241:H513–H518.

Ham KN, Hurley JV, Ryan GB, Storey E. Localization of particulate carbon in metaphyseal vessels of growing rats. Aust J Exp Biol and Med Sci. 1965; 43:625–638. [PubMed: 5845598]

Hansson LI. Daily growth in length of diaphysis measured by oxytetracycline in rabbit normally and after medullary plugging. Acta Orthop Scand Suppl. 1967; 101:1–199.

Heinzman U. FITC-dextrans as fluorescence and electron microscopic tracers in studies on capillary and cell permeability of the CNS. Experientia. 1980; 36:885–887. [PubMed: 6156860]

Horton WA. Skeletal development: insights from targeting the mouse genome. Lancet. 2003; 362:560–569. [PubMed: 12932391]

Hunter WL, Arsenault AL. Vascular invasion of the epiphyseal growth plate: analysis of metaphyseal capillary ultrastructure and growth dynamics. Anat Rec. 1990; 227:223–231. [PubMed: 2350011]

Hunziker EB, Schenk RK. Physiological mechanisms adopted by chondrocytes in regulating longitudinal bone growth in rats. J Physiol. 1989; 414:55–71. [PubMed: 2607442]

Irving MH. The blood supply of the growth cartilage in young rats. J Anat London. 1964; 98:631–639. [PubMed: 14229993]

Kamler M, Pixanis N, Hagl S, Gebhard MM, Jakob H. Extracorporal circulation-induced leukocyte/endothelial cell interaction is inhibited by dextran. Clin Hemorheol and Microcirc. 2004; 31:139–148.

Karsenty G. Chondrogenesis just ain't what it used to be! J Clin Invest. 2001; 107:405–407. [PubMed: 11181639]

Kloppenburg P, Zipfel WR, Webb WW, Harris-Warrick RM. Highly localized Ca(2+) accumulation revealed by multiphoton microscopy in an identified motoneuron and its modulation by dopamine. J Neurosci. 2000; 20:2523–33. [PubMed: 10729332]

Komuta K, Hirano T, Iwasaki K. Structural changes in blood vessels entering the growth plate during growth in rats. Int Orthop (SICOT). 1998; 22:11–18.

Kronenberg HM. Developmental regulation of the growth plate. Nature. 2003; 423:332–336. [PubMed: 12748651]

Kuettner, KE.; Pauli, BU. Cartilage: Structure, Function and Biochemistry. Vol. 1. New York: Academic Press; 1983. Vascularity of cartilage; p. 281-312.

Long F, Linsenmayer TF. Regulation of growth region cartilage proliferation and differentiation by perichondrium. Development. 1998; 125:1067–1073. [PubMed: 9463353]

McLean W, Olsen BR. Mouse models of abnormal skeletal development and homeostasis. Trends Genet. 2001; 17:S38–S43. [PubMed: 11585675]

Melrose J, Smith S, Whitelock J. Perlecan immunolocalizes to perichondrial vessels and canals in human fetal cartilaginous primordia in early vascular and matrix remodeling events associated with diarthrodial joint development. J Histochem Cytochem. 2004; 52:1405–1413. [PubMed: 15505335]

Mertz J. Nonlinear microscopy: new techniques and applications. Curr Opin Neuro. 2004; 14:610–616.

Michel CC, Curry FE. Microvascular permeability. Physiol Rev. 1999; 79:703–761. [PubMed: 10390517]

Miller JC, Pien HH, Sahani D, Sorensen AG, Thrall JH. Imaging angiogenesis: applications and potential for drug development. J Natl Cancer Inst. 2005; 97:172–187. [PubMed: 15687360]

Morgan JD. Blood supply of growing rabbit's tibia. J Bone Joint Surg. 1959; 41-B:185–203.

Niell CM, Smith SJ. Live optical imaging of nervous system development. Annu Rev Physiol. 2004; 66:771–798. [PubMed: 14977421]

Okazaki K, Sandell LJ. Extracellular matrix gene regulation. Clin Orthop Relat R. 2004; 427S:S123–S128.

Ortega N, Behonick DJ, Werb Z. Matrix remolding during endochondral ossification. Trends Cell Biol. 2004; 14:86–93. [PubMed: 15102440]

Pateder DB, Rosier RN, Schwarz EM, Reynolds PR, Puzas JE, D'Souza M, O'Keefe RJ. PTHrP expression in chondrocytes, regulation by TGF-beta, and interactions between epiphyseal and growth plate chondrocytes. Exp Cell Res. 2000; 256:555–562. [PubMed: 10772827]

Pathi S, Rutenberg JB, Johnson RL, Vortkamp A. Interaction of Ihh and BMP/Noggin signaling during cartilage differentiation. Dev Bio. 1999; 209:239–253. [PubMed: 10328918]

Pearson MJ, Lipowsky HH. Influence of erythrocyte aggregation on leukocyte margination in postcapillary venules of rat mesentery. Am J Physiol Heart Circ Physiol. 2000; 279:H1460–H1471. [PubMed: 11009430]

Predescu SA, Predescu DN, Palade GE. Plasmalemmal vesicles function as transcytotic carriers for small proteins in the continuous endothelium. Am J Physiol. 1997; 272:H937–H949. [PubMed: 9124458]

Ranvier, L. Traité Technique D'Histologiem. Paris: Librairie F. Savy; 1889. Development du tissu osseux; p. 340-363.

Roberts WG, Palade GE. Increased microvascular permeability and endothelial fenestration induced by vascular endothelial growth factor. J Cell Sci. 1995; 108:2369–2379. [PubMed: 7673356]

Rubart M. Two-photon microscopy of cells and tissue. Circ Res. 2004; 95:1154–1166. [PubMed: 15591237]

Schubert W, Frank PG, Razani B, Park DS, Chow C, Lisanti MP. Caveolae-deficient endothelial cells show defects in the uptake and transport of albumin in vivo. J Biol Chem. 2001; 276:48619–48622. [PubMed: 11689550]

Silverstein, RL. The Vascular Endothelium. In: Gallin, JI.; Snyderman, R., editors. Inflammation: Basic Principles and Clinical Correlates. 3rd. Philadelphia: Lippincott Williams & Wilkins; 1999. p. 207-225.

Simionescu N, Simionescu M, Palade GE. Permeability of intestinal capillaries: Pathway followed by dextrans and glycogens. J Cell Biol. 1972; 53:365–392. [PubMed: 4112540]

Simionescu M, Gafencu A, Antohe F. Transcytosis of plasma macromolecules in endothelial cells: a cell biological survey. Microsc Res Tech. 2002; 57:269–288. [PubMed: 12112439]

Smart EJ, Graf GA, McNiven MA, Sessa WC, Engelman JA, Scherer PE, Okamoto T, Lisanti MP. Minireview: Caveolins, liquid-ordered domains, and signal transduction. Molec Cell Biol. 1999; 19:7289–7304. [PubMed: 10523618]

Stanka P, Bellack U, Lindner A. On the morphology of the terminal microvasculature during endochondral ossification in rats. Bone Miner. 1991; 13:93–101. [PubMed: 1711906]

Thorball N. FITC-dextran tracers in microcirculatory and permeability studies using combined fluorescence stereo microscopy, fluorescence light microscopy and electron microscopy. Histochemistry. 1981; 71:209–233. [PubMed: 6165704]

Trueta J. The role of the vessals in osteogenesis. J Bone Joint Surg. 1963; 45-B:402–418.

Trueta, J. Studies of the Development and Decay of the Human Frame. London: William Heinemann Medical Books LTD; 1968. The effect of ischaemia on the epiphyseal cartilage; p. 108-117.

Tsai AG, Johnson PC, Intaglietta M. Oxygen gradients in the microcirculation. Physiol Rev. 2003; 83:933–963. [PubMed: 12843412]

Volk SW, Leboy PS. Regulating the regulators of chondrocyte hypertrophy. J Bone Miner Res. 1999; 14:483–486. [PubMed: 10234568]

Vortkamp A, Lee K, Lanske B, Segre GV, Kronenberg HM, Tabin CJ. Regulation of rate of cartilage differentiation by Indian hedgehog and PTH-related protein. Science. 1996; 273:613–622. [PubMed: 8662546]

Vu TH, Shipley JM, Bergers G, Berger JE, Helms JA, Hanahan D, Shapiro SD, Senior RM, Werb Z. MMP-9/gelatinase B is a key regulator of growth plate angiogenesis and apoptosis of hypertrophic chondrocytes. Cell. 1998; 93:411–22. [PubMed: 9590175]

Williams RM, Zipfel WR, Webb WW. Multiphoton microscopy in biological research. Curr Opin Chem Biol. 2001; 5:603–608. [PubMed: 11578936]

Xu C, Zipfel W, Shear JB, Williams RM, Webb WW. Multiphoton fluorescence excitation: new spectral windows for biological nonlinear microscopy. Proc Natl Acad Sci USA. 1996; 93:10763–8. [PubMed: 8855254]

Zelzer E, McLean W, Ng YS, Fukai N, Reginato AM, Lovejoy S, D'Amore PA, Olsen BR. Skeletal defects in VEGF (120/120) mice reveal multiple roles for VEGF in skeletogenesis. Development. 2002; 129:1893–1904. [PubMed: 11934855]

Zelzer E, Olsen BR. Multiple roles of vascular endothelial growth factor (VEGF) in skeletal development, growth, and repair. Curr Topics Dev Biol. 2005; 65:169–187.

Zipfel WR, Williams RM, Christie R, Nikitin AY, Hyman BT, Webb WW. Live tissue intrinsic emission microscopy using multiphoton-excited native fluorescence and second harmonic generation. Proc Natl Acad Sci USA. 2003a; 100:7075–7080. [PubMed: 12756303]

Zipfel WR, Williams RM, Webb WW. Nonlinear magic: multiphoton microscopy in the biosciences. Nat Biotechnol. 2003b; 21:1369–1377. [PubMed: 14595365]

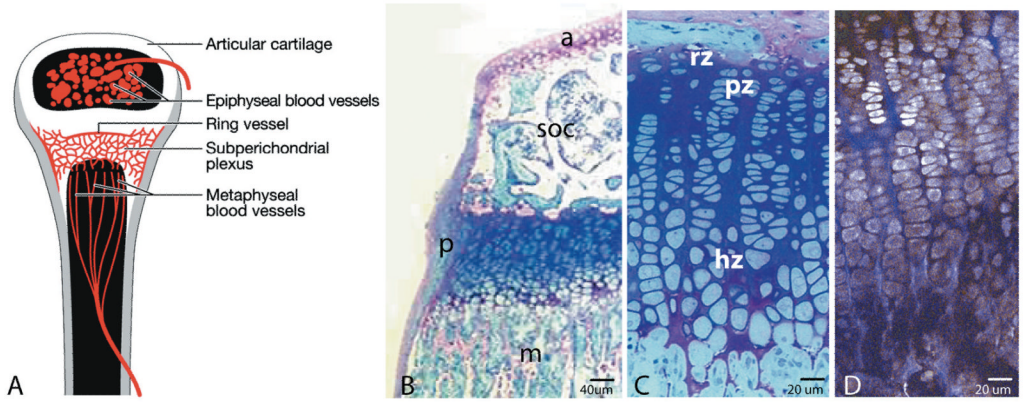

Figure 1.

Figure 1A depicts the proximal tibia in a young mouse showing the three potential routes of vascular access to the growth plate: vessels of the epiphysis, vessels of the metaphysis, and vessels associated with a ring vessel and plexus running just deep to the periosteum. The latter vessels would not be visible on a sagittal section, since they are associated with the periosteum. Figure 1B is a one-micron-thick histological section of the proximal tibia from a four-week-old mouse, fixed in 2% paraformaldehyde/ 2% glutaraldehyde with 0.7% ruthenium hexamine trichloride, embedded in Epon-Araldite (Hunziker and Schenck, 1989), and stained with methylene blue/azure II/basic fuchsin. Note the articular cartilage (a), trabecular bone of the secondary center of ossification (soc), the perichondrium (p), and the longitudinally oriented bone of the elongating metaphysis (m). As shown in C, the reserve cell zone (rz) is limited to one or two cells adjacent to the secondary center. Proliferative zone cells (pz) are arranged in columns with their long axis perpendicular to the direction of growth; hypertrophic zone cells (hz) have their long axis parallel to the direction of elongation. Figure 1D is a multiphoton image of a sagittally sectioned, freshly isolated growth plate, non-stained, showing the same cellular morphology. Cellular autofluorescence (grey pseudocolor) and collagen second harmonic generation (blue pseudocolor) can be seen when the section is illuminated at 770 nm.

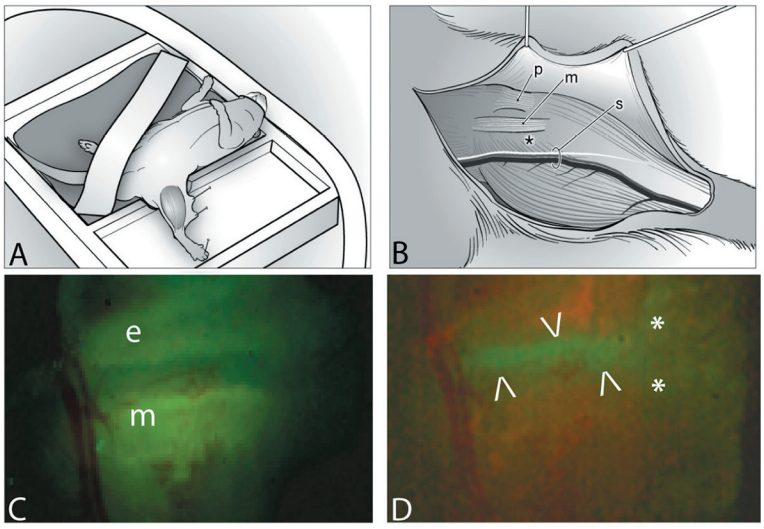

Figure 2.

For surgery and imaging the mouse was positioned in dorsal recumbency, on a heating pad under isoflurane anaesthesia (A). A surgical approach was made to the medial side of the left tibia using the patellar ligament (p), the medial collateral ligament (m) and the saphenous vessels and nerve (s) as landmarks (B). An asterisk (*) indicates the position of the growth plate with the perichondrium intact. The surgical field is illuminated to demonstrate the yellow-green fluorescence of OTC in the epiphyseal (e) and metaphyseal (m) bone (C). The growth plate appears as a non-fluorescent band between the two areas of fluorescing bone. Figure 2D is the identical surgical field, illuminated to show the green fluorescence of the GFP-positive chondrocytes of the growth plate, between the arrowheads. Asterisks mark the medial collateral ligament.

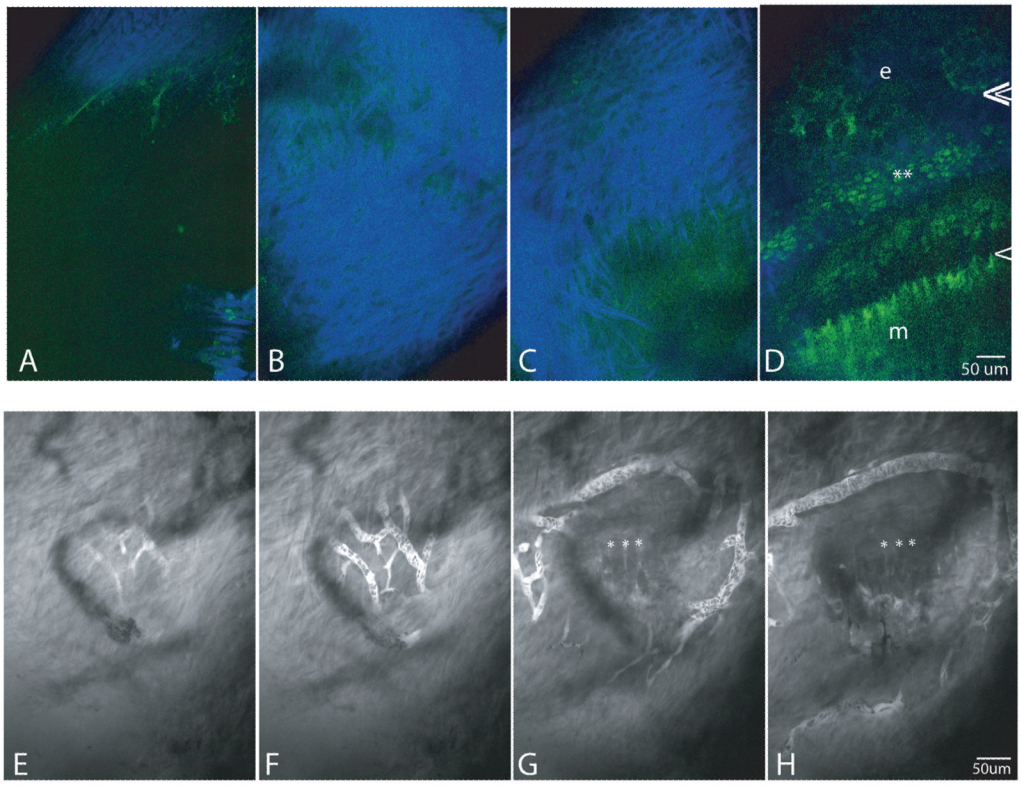

Figure 3.

Figures A-D are four frames of a z-series, from superficial to the periosteum (A), through the periosteum (B,C), and to the growth plate (D) to verify orientation and positioning. Separation of emission colors allows simultaneous imaging of collagen second harmonic generation (blue), and OTC and GFP-fluorescence (green). GFP-positive proliferative cells are adjacent to the asterisks. OTC-fluorescent epiphyseal and metaphyseal COJs are indicated by double and single arrowheads respectively. The growth plate as imaged in Figure D is 70μm deep to the perichondrium. e=epiphyseal bone; m=metaphyseal bone Figures 3. E-H demonstrate the network of the vascular plexus, visualized after an IP injection of fluorescein so that the plasma is fluorescent and blood cells can be seen as dark shadows within the vessels. Frames E and F (taken 5 μm deeper than E), demonstrate that the network of the plexus is on the deep side of the collagen of the perichondrium, and that the ring vessel is in a plane slightly deeper than the plexus. In frames G (another 20 μm deeper) and H (another 10 μm deeper) asterisks are positioned at the metaphyseal COJ. The ring vessel encircles the growth plate at approximately the P/H junction, and the plexus extends entirely on the hypertrophic zone side.

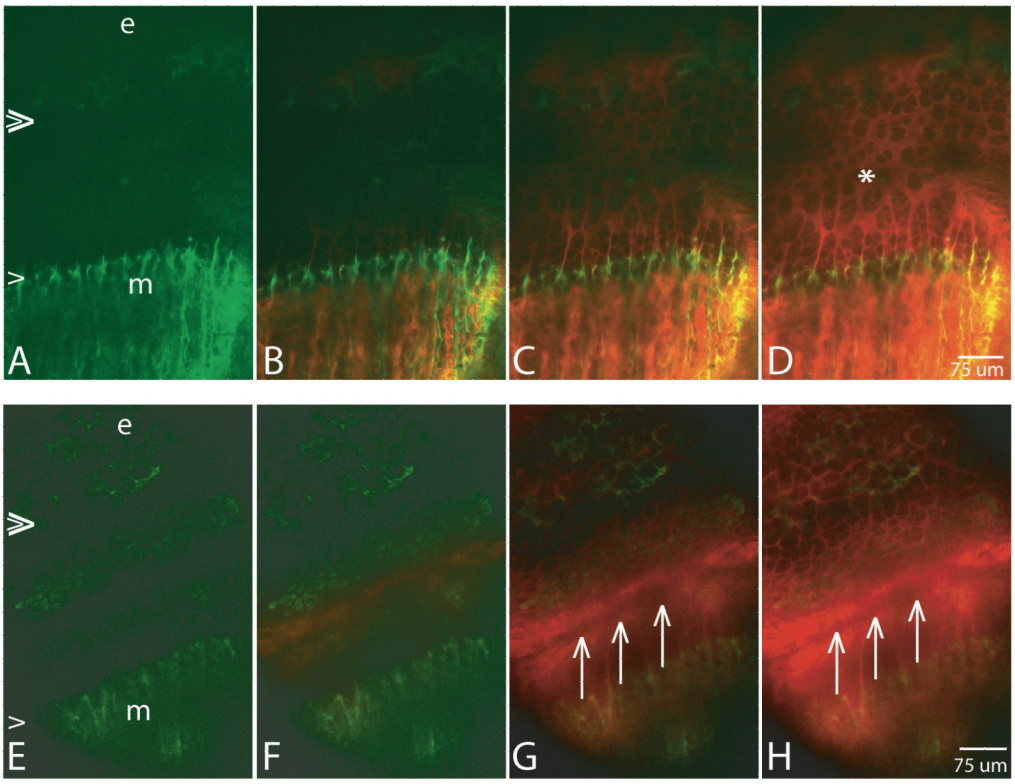

Figure 4.

Each row shows four frames from a timed series after injection of fluorescein (vascular concentration ~2 mM), IP, pseudo-colored in red. The pattern of arrival of fluorescein into the growth plate reflects the depth of the imaging plane relative to ring vessel and plexus, more superficial in frames E-H than in frames A-D. The epiphyseal COJ is indicated by double arrowheads at the left in A and E, the metaphyseal COJ by a single arrowhead, and OTC-labeling of the bone is green. e=epiphyseal bone; m=metaphsyeal bone. In series A-D from a GFP-/- mouse, fluorescein arrives essentially simultaneously into the growth plate from both the epiphyseal and the metaphyseal sides (C, D are 336 and 590 seconds after injection, respectively), and the last area of the growth plate to be reached is the P/H junction (asterisk). By contrast, in a more superficial focal plane shown in E-H from a GFP +/- mouse, the P/H junction is the first region to receive fluorescein (F and continuing into G and H). Times after injection for F,G,H are 94, 242, and 401 seconds, respectively. The shadow indicated by three arrows in G and H is that of the ring vessel, with intense fluorescein on either side.

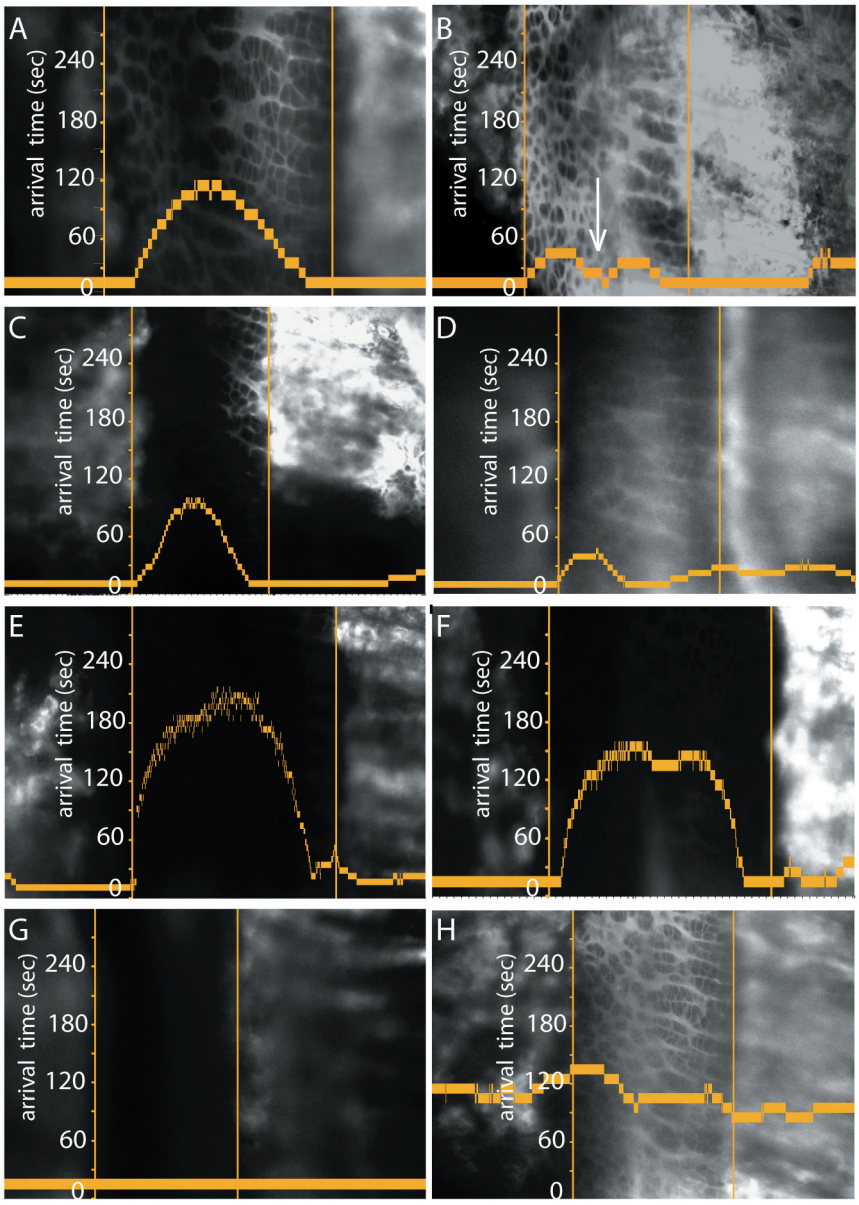

Figure 5.

Graphs show tracer arrival half-time (vertical axis) relative to the tracer's position-specific fluorescence at five minutes. The epiphyseal bone is on the left and the metaphyseal bone on the right, with the respective COJs represented as vertical lines. Figures A,B plot the entrance of fluorescein (~2 mM vascular concentration), in a relatively deep (A, 90 μm deep to the periosteum) versus a relatively superficial (B, 45 μm deep to the periosteum) position. In the deep location (A), tracer arrives first from both COJ vasculatures, whereas in the superficial position arrival occurs just as early at the P/H junction, presumably from the ring vessel and plexus (arrow in B). Figures C,D and E,F are analogous graphs for the entrance of 3 kDa and 10 kDa dextrans, respectively, after IC injection of 50μl, 0.1% solution. Patterns of arrival are identical to those for fluorescein. Figure G demonstrates that the 40 kDa dextran, injected IC, does not enter the growth plate. Figure H demonstrates an IP injection of fluorescein (200μl, 0.5% solution) in a superficial position. The form of the graph indicates the arrival of fluorescein to the growth plate is significantly slower than

when injected IC (B), and also that in this image plane a significant amount is reaching the hypertrophic zone from the plexus, indicated by the relatively long straight line in the graph covering most of the hypertrophic cell zone.

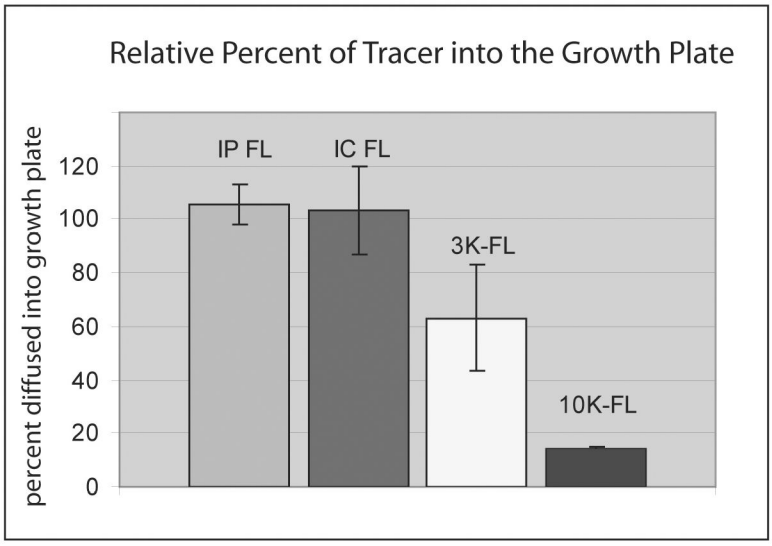

Figure 6.
This bar graph presents data for estimating the relative amount of tracer that leaves the vasculature and enters the growth plate. Data are calculated as the ratio of fluorescence intensity in the growth plate relative to the maximal vascular fluorescence. Both IC and IP fluorescein enter the growth plate readily from the vasculature and to the same extents. By contrast, entrance of the 3 kDa dextran is half that compared to fluorescein, and the 10 kDa dextran only one tenth.

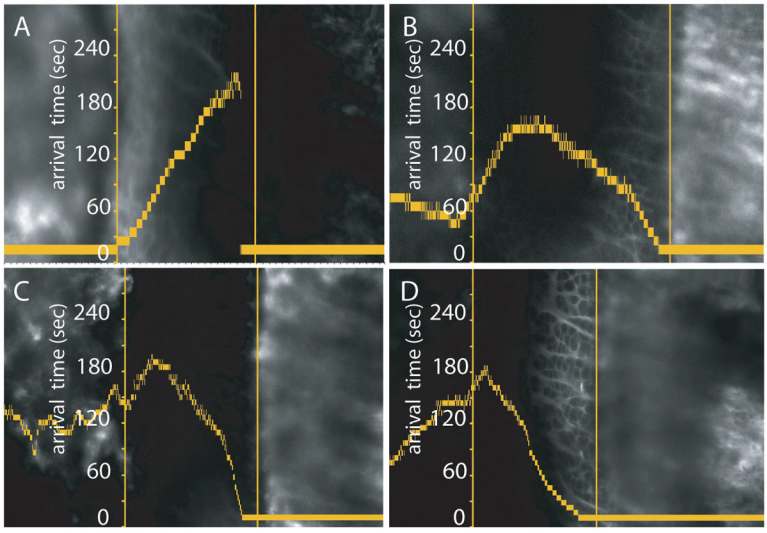

Figure 7.

These graphs are presented with the same conventions as Figure 5. Figures A,B demonstrate that IC-injected fluorescein (50μl, 1% solution) can enter entirely from the epiphyseal vasculature (A), or almost entirely from the metaphyseal vasculature (B), if the experimental situation is such that the vasculature of one side of the growth plate fills more rapidly than that of the other. In this situation, the fluorescein that enters has the potential to move throughout the growth plate, reaching the opposite COJ (7A). Figure 7C demonstrates that dextrans also behave this way. The specific graph demonstrates entrance of a 10 kDa dextran, primarily from the metaphyseal side and diffusing from the metaphyseal COJ well into the proliferative cell zone. Figure 7D is an IC injection of fluorescein, following the 10 kDa injection, demonstrating that directionality of entrance of fluorescein mirrors that of the 10 kDa dextran.